Research Article

About Fireflies and Science

Gian Carlo Montanari[1,*] and Robert Hebner[2]

[1]*Center for Advanced Power Systems (CAPS), Florida State University, USA*
[2]*Center for Electromechanics (CEM), The University of Texas at Austin, USA*

___

Abstract

We are enlightened by problems to solve and ideas, which sometimes last until we understand and then switch off too soon. We try to capture entanglements of a much more complex phenomenology than the bits we can understand and make use for the advancement of science and technology. Frustration is the partner of our life, but lights and dreams make us struggle to keep the light alive. Catching fireflies is our dream and our doom.

Keywords: Dielectric, nanoparticles, superconductivity, thermal conductivity

___

1. Introduction

When we think of Toshikatsu Tanaka, his scientific contributions and the many conferences spent together come to mind. However, one of the authors of this paper, Gian Carlo Montanari (GC), has one particularly vivid memory of Prof. Tanaka. Many years ago, Toshikatsu and his wife were walking from a restaurant to GC's home in the Bologna hills, in the countryside. Toshikatsu was trying to catch fireflies to show to his wife. He said that they were a memory from his youth, because step-by-step they disappeared from the places he was living in Japan.

In many ways, catching fireflies an apt metaphor for a scientist's life. This is what many of us, and certainly Toshikatsu, have done for most of our life, trying to discover a spark of insight while exploring the darkness of unexplained phenomena. We seldom catch a firefly, but the reward is worth the effort.

This paper describes a few firefly cases in the energy field: the light of possibility, the dark of research, the light of light of resolved issues. The areas of focus are superconducting materials and nanomaterials. These are two areas in which Dr. Tanaka made important contributions.

Superconducting materials offer great promise to improve the delivery of electrical energy. Referring to cables, the promise is the ability to achieve extremely large specific energy transmission with low losses. However, it was discovered the initial superconducting tapes used for cable conductors were mechanically weak, dimming hopes for the technology. In response, the research community developed a nonmagnetic metal cladding to achieve long term stability and reliability of the superconducting strip, turning on again the light of opportunities related to superconductivity.

Nanostructured materials promised the capability to design a material with properties that did not occur in nature. As regards dielectric materials, the light of enthusiasm was often dimmed by experimental results showing contrasting indications of the type of electrical insulation properties that could be improved by the introduction of nanoparticles. The explanation of the pʾEhysics behind the functionality of nanoparticles in dielectrics helped to tune particle type, size and treatment to improve specific dielectric properties. These two topics are discussed in the following sections, highlighting the firefly paradigm.

2. Superconductive tapes

The development in the 1990's of high-temperature superconductors (HTSC), especially BSCCO multifilamentary tapes, was the light of a firefly. It provided the technology for manufacturing of tapes thousand meters long, with an ampacity of the order of 20,000-30,000 A/cm^2 and critical temperatures higher than liquid nitrogen (much higher than those of metallic, Type 1, superconductors), [1-3]. Application to power cables, for new transmission systems or for refurbishing existing ones, increasing the power, was one of an exciting perspective of BSCCO discovery (awarded by the Nobel price, Bednorz and Muller, 1986), [4-6].

However, multifilamentary tapes in cables are subjected to mechanical stresses (bending, tensile) and strain, especially for large power and e.g. submarine cables. The superconductor tape structure was composed by multiple filaments embedded in an Ag tube, which was expected to also provide the needed mechanical strength to the assembly. Before any implementation of the technology could be considered, it was necessary to check experimentally and model the endurance to mechanical stress and strain. This is because the long-term performance and reliability of the new technology were totally unknown.

Since mechanical failure is a "weak link" type failure, researchers characterized the mechanical influence on the critical current of multifilamentary superconductive tapes by the Weibull distribution. Accelerated life tests under mechanical stress and strain, were conducted until the critical current density reached a fixed end point. V-I characteristic measurements were performed at different times during aging tests, in order to plot the relevant Weibull graphs and extract the behavior of the Weibull parameters as a function of aging.

The ultimate rationale for the use of the Weibull distribution to process critical current values comes from the fact that experimental voltage-current (V-I), or electric field-current density (E-J) characteristics of a type-II superconductor (SC-II), generally do not fit the shape expected according to the flux-flow theory, due to scatter of local values of critical current density, J_c, [7]. Indeed, each section of a SC-II material starts transition at different values of critical current density, J_c [8, 9]. To model this behavior, a probability function, g(J), was introduced, which describes the probability that a section of a superconductor has a given value of J_c. Its integration, which corresponds to the cumulative probability, G(J,), can be approximated by a two-parameters Weibull distribution, [10, 11], which fits both skewed and unskewed probability density characteristics:

$$F(x) = 1 - exp[-(x/\alpha)\beta]$$ (1)

Where α and β are scale and shape parameters, whereas the random variable, x, corresponds to the critical current density, J_c [12]. Examples of V-I characteristics measured in unaged and aged specimens (not pretending to separate the contribution of silver support) are reported in Fig. 1 (relevant to subjected to accelerated mechanical aging, under vibration). The silver shield V-I characteristic is also reported, for the sake of comparison. It comes out clearly that aging can significantly affect V-I characteristics and that V-I curves tend to the silver resistance for values of current progressively decreasing as aging time increases.
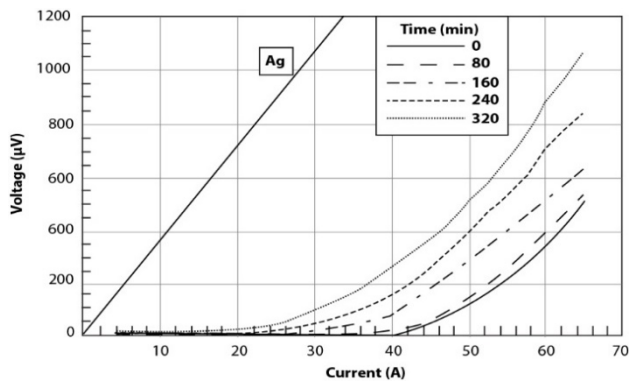

Fig. 1. V-I characteristics at different aging times for accelerated vibration aging. After [12].

This reflects into the Weibull distributions of the critical current of Fig. 2. Plotting the Weibull distribution parameters, α and β, as a function of aging time, Fig. 3, it comes out clearly that with mechanical aging the critical current density falls and its dispersion increases (β decreases), that supports the chaotic and inhomogeneous behavior of the degradation process. Similar, and even more dramatic, effects are obtained with tensile stress and strain, which dimmed the light shed by the discovery and manufacturing of BSCCO tapes for power cable applications.

The light brightened again when, based on such results, the use of a further mechanical support, made by a cladding of a nonmagnetic steel, was implemented, see Fig. 4. The critical current density decline was significantly improved, for vibration, and tensile stress, as well as tensile strain. This is highlighted by the values of the scale parameter of the relative critical current density Weibull function reported in Fig. 5, where non-reinforced tapes are compared with nonmagnetic-steel reinforced tapes, [13]. To investigate the potential effect of such amelioration on tape life, accelerated life tests were carried out on tape specimens, fitting to the so-called inverse power model (IPM), [14]:

$$t_F = kS^{-n}$$ (2)

Where t_F is failure time (time to reach the fixed endpoint), S is applied tensile stress; k and n are the model parameters.
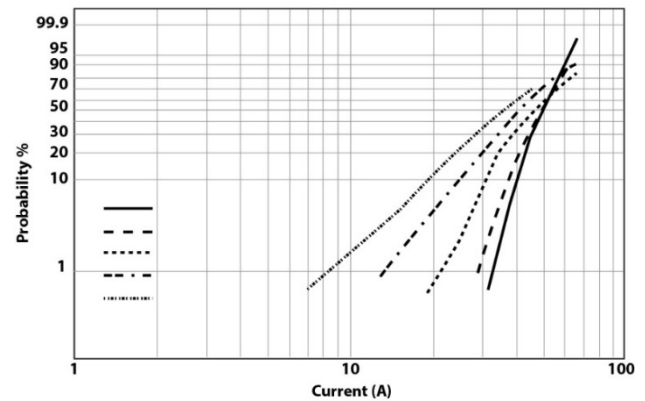

Fig. 2. Weibull plots derived from normalized prime derivative (Fig. 3A) at different aging times for accelerated vibration aging.
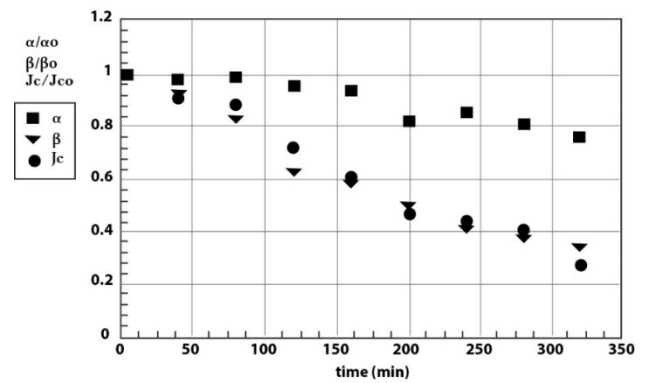

Fig. 3. Time behavior of relative values of scale (α) and shape (β) parameters of the Weibull distribution, as well as of critical current density, J_c for accelerated vibration aging. The reference value for α and shape β are those relevant to unaged specimens.
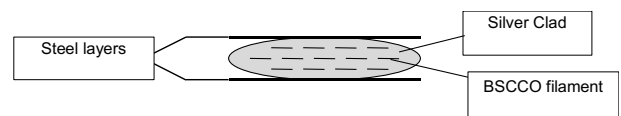

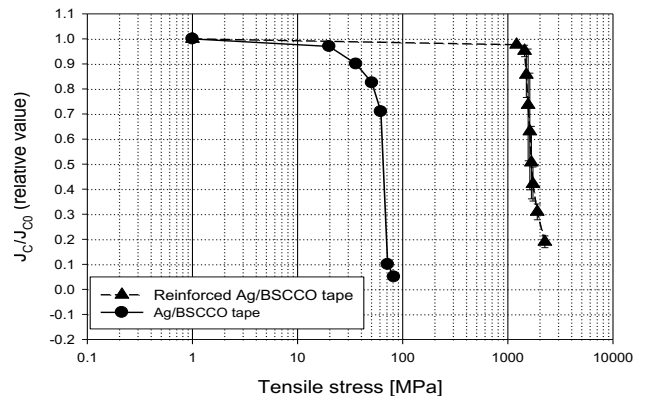**Fig. 4.** Structure of the BSCCO-Ag steel-reinforced tape.


Fig. 5. Example of relative critical current density (scale parameter of the Weibull distribution) as a function of tensile strain amplitude for conventional and steel-reinforced specimens. Confidence intervals are relevant to 95% probability.

This latter is called *endurance coefficient*, which provides a measure of the capability of a material/system to withstand the stress (the larger *n*, the stronger the material/system) [14]. This life model, which is linear on log-log plot, provides insight into the effect of mechanical stress on long-term performance of HTSC steel-reinforced tape, especially in comparison with previous HTSC tape configurations. As such, it constitutes a basis for a probabilistic design of the HTSC cable, providing a relationship relating life to mechanical stress. Fig. 6 shows results of accelerated life tests under tensile stress (they are processed by Eq. 1 relevant to failure times, and considering, in the Fig., probability 63.2%). As can be seen, life test results indicate that both life percentiles and the voltage endurance coefficient increase dramatically. Additional losses introduced by the reinforcement were the measured and compared to those of the DSCII superconducting material, reaching a good equilibrium and design feasibility [15].

The above research work opened the door to the possibility to designing and manufacturing superconducting cables, switching on the lost light. Installation of HV SC cable were in fact, realized in early 2000
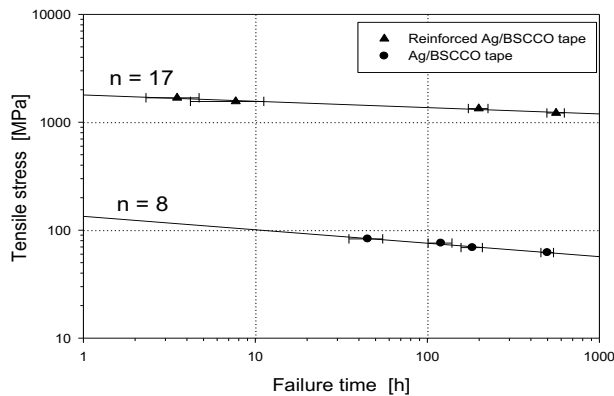
Fig. 6. Life test results at probability 63.2% performed under tensile strain on conventional and steel-reinforced tapes. Lifelines and endurance coefficient values are also reported. Confidence intervals are relevant to 95% probability.
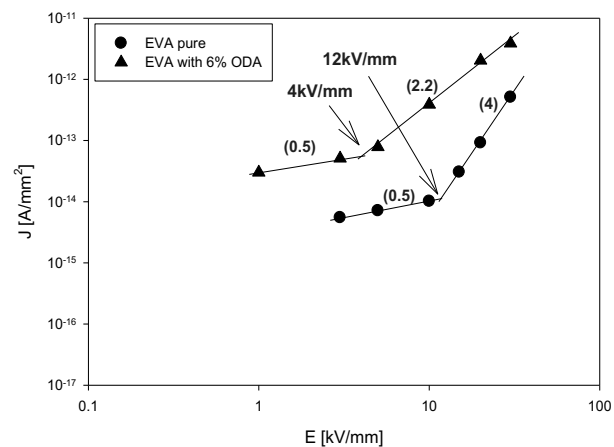

Fig. 7. Quasi steady-state current density as a function of poling field for Ethylene-Vinyl acetate, EVA, pure and filled 6%. The threshold for the onset of SCLC conduction mechanism is indicated by an arrow. Filler: synthetic fluorohectorite modified by protonated octadecyl amine NH_3^+ (ODA).

3. Nanostructured dielectrics

Another epochal event with the potential to significantly influence the field of energy and electrified transportation is the advent of nanotechnology (Nobel price 2007 to Albert

Fert, Peter Grunberg). In the early 2000's several papers began to report results of research activity related to the use of nanostructured dielectrics for electrical insulation. The trend was to deliver the enthusiastic message that whatever nano-powder could improve electrical, thermal and mechanical dielectric properties [16-27]. The light was shining and stimulating enthusiastic research, but it soon became obvious that often contrasting results were achieved with nano-structuration of dielectric materials. Sometimes it was found that e.g. dissipation factor and conductivity were decreasing, sometimes the opposite, Fig. 7. The same was true for breakdown voltage, BV, Fig. 8, space charge and other electrical properties [22]. PD resistance could sometimes be improved, Fig. 9 [28], but other times nanofilling had no effect. This was rapidly generating confusion as a whole, dimming the light. The firefly was losing energy and momentum. That was the time when science had to guide experiments, discovering the reasons behind the contrasting results and the direction to take to make use of this revolutionary technology also in the field of electrical insulation.

The conclusions in [23], summarized and complemented below, may constitute an example on how to develop some scientific explanation of the contradictory results.
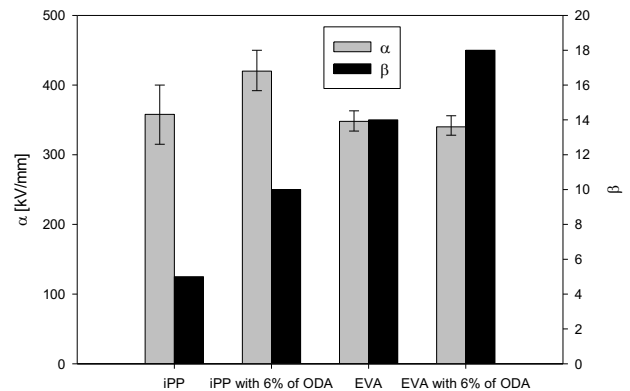
Fig. 8. Scale and shape parameter values obtained from the Weibull distribution of breakdown voltage for both polypropylene, PP, and ethylene vinyl acetate, EVA, pure and filled (6%). The confidence intervals at probability 95% are indicated. Filler: synthetic fluorohectorite modified by protonated octadecyl amine NH_3^+ (ODA).
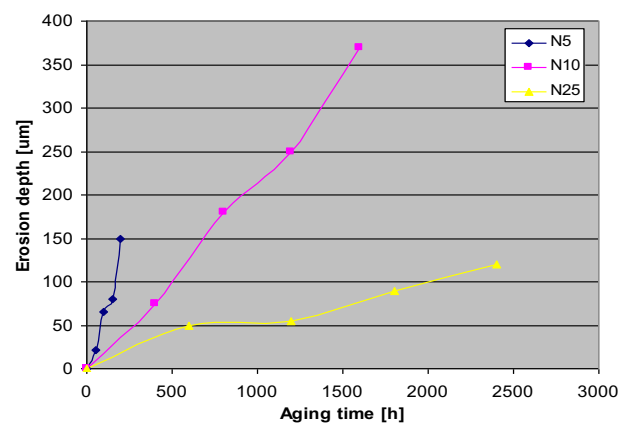
Fig. 9. Erosion depth (A) and area (B) as a function of aging time for the three tested materials. Epoxy-resin filled with spherical nano-silicates, density from 5% to 25% in weight.

4. Effects of nanomization

(1) DC conductivity increases or decreases depending on

measurement conditions and type of nanofillers.

(2) Interfacial polarization can be reduced compared to microcomposites.

(3) There seems to be a reduction of permittivity due to nanomization. But change of permittivity as well as tan δ is complicated, and not conclusive: it is questionable whether the permittivity and tan δ are reduced by nanomization at the commercial frequency.

(4) Space charge, TSC (thermally stimulated currents) and EL (electroluminescence) also give complex results in their threshold field and quantity. Introduction of additional levels of shallow and deep traps, as well increase of trap density, might be involved. These might be related to "interaction zones" [18]. It is therefore necessary to characterize the interaction zones between nanofillers and polymer matrices chemically and physically (note: see e.g. the work done later by T. Tanaka [29]).

(5) PD and tracking resistance improve. The role of nanofillers type and shape and the effect of interaction zones while promising, requires clarification.

(6) Thermal conductivity, temperature index and glass transition temperature can be increased by proper selection of nanofiller [19, 30].
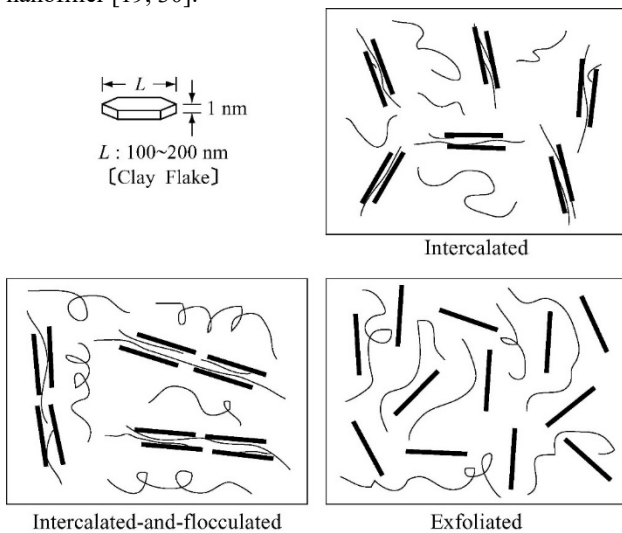
The predominant effect of interfaces between nanoparticles and dielectric was theorized and modelled, [29, 31]. The effect of particle dispersion, aspect ratio and water content explained, and it was a significant contributor to the explanation of contrasting experimental results. Large aspect ratio particles could, e.g., improve PD resistance and mechanical properties, but worsen space charge conductivity and losses due also to the larger capability to attract moisture [31-34].

The need for functionalization, especially in clays that must be intercalated (exfoliated) by polymer chains to increase the interface extent and avoid agglomeration, [23, 35] and Fig. 10 and Fig. 11, were singled out, for example, as a potential week point as regards electrical properties. Metal oxide, as SiO_2 nanoparticles, may require functionalization to improve interface interactions with polymers, but there is no need to modify the intrinsic particle structure as for exfoliation of silica, [19, 23,36, 37], Fig. 12. In addition, there is much less propensity to agglomerate, [37], and attract water at interfaces, going towards potential percolation paths that can affect dramatically electrical properties [34, 38].

Fig. 12. Example of the morphology of the interface Polymer/ Metal Oxides.

Fig. 10. Schematic illustration of three different types of polymer/layered silicate nanocomposites.
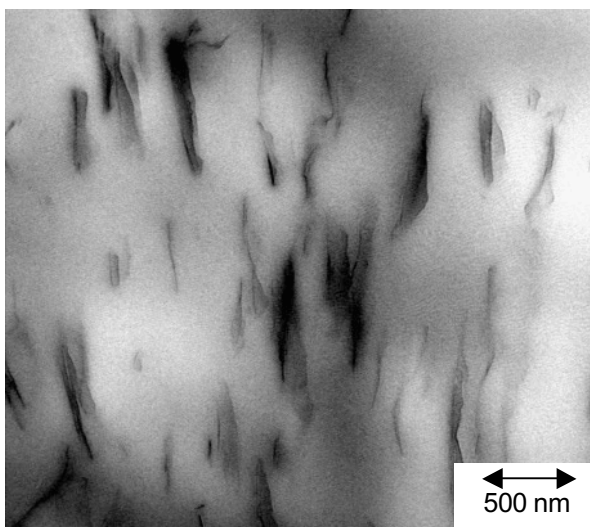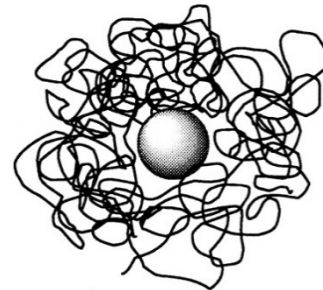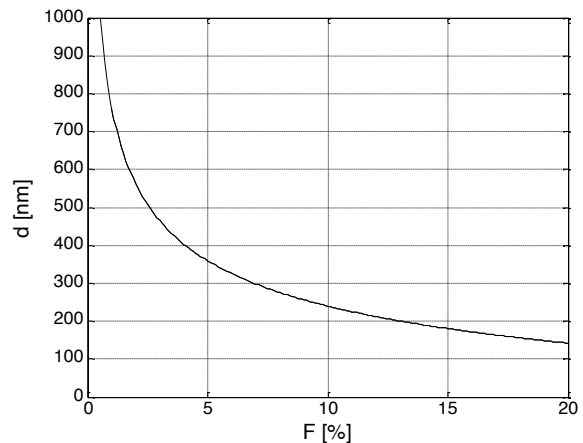
b) iPP nanocomposite

Fig. 11. TEM micrographs of PP compound containing 6 wt.-% of modified organohectorite and 20 wt.-% of the PP-g-MA compatibilizer.

Fig. 13. Average distance between filler particles, calculated according to (3) (ρ_f=3000g/l, ρ_m=1400g/l, r=100 nm), as a function of nano-particle concentration; spherical particles, Eq. (4).

This aspect was modelled based on particle dimensions, aspect ratio and treatment. The mechanism by which a given amount of adsorbed water gives rise to different modifications of the dielectric behavior of composites with different filler particle shapes was explained through considerations regarding the average distance among filler particles. In order to evaluate the average distance among the nano-particles when they are dispersed in the polymer matrix, a low aspect ratio nanoparticle (e.g. boehmite, SiO_2) can be roughly considered as made by spherical particles having constant

radius, r, uniformly dispersed in a homogeneous and isotropic polymeric matrix. Hence, the number of particles per unit volume of the nanocomposite, N, is:

$$N = \frac{M_f}{\frac{4\pi}{3}\rho_f r^3} \qquad (3)$$

Where M_f is the mass of the filler per unit volume. The average interparticle distance, d, can be obtained by [34, 39]:

$$d = r \cdot \left\{ \left[\frac{4\pi}{3} \left(1 + \frac{1-F}{F} \frac{\rho_f}{\rho_m} \right) \right]^{\frac{1}{3}} - 2 \right\}; \qquad (4)$$

Where F is the filler concentration (wt. %), ρ_f and ρ_m are filler and matrix densities. In the case of spherical particles, with an average radius of 100 nm, the average distance is reported in Fig. 13, as a function of the filler concentration (%wt). For a filler concentration of 5 % wt (at which we can observe, in general, the best improvement of electrical properties, if any) the average distance among the particles is about 360 nm with a number of particles per cubic meter of $5.6 \cdot 10^{18}$. Assuming that contamination, e.g. the water, is located in a spherical shell around each filler particle, the thickness of the water shell, Δr, can be obtained from the water shell volume, ΔV, which depends on water adsorption:

$$\Delta r = \sqrt[3]{\frac{3}{4\pi}\Delta V + r^3} - r \qquad (5)$$

The thickness of the water shell results about 3 nm in the case of spherical particles and for the maximum water adsorption level measured in the nanocomposite (1500 ppm). This value is much smaller than the average distance among the particles. In this way a moderate amount of adsorbed water (a preliminary drying treatment was performed on all the used filler) does not lead to the formation of percolative paths and the dielectric properties should not be affected significantly (if not, mildly, those associated to trapping states). Drying treatments, in this case, will not change noticeably the properties of the composite.

In the case of high aspect ratio nanoparticles, e.g. lamellar silicates, the number of the particles per unit volume of the nanocomposite can be obtained by (assuming uniform distribution):

$$N = \frac{M_f}{\rho_f V_p} \qquad (6)$$

Where V_p is the volume of the single particle. The volume of a particle, after dispersion in the polymer matrix, can be evaluated on the basis of the average particle dimensions, assuming for a lamella the shape of a parallelepiped with height l and thickness d_l (being l/d_i the aspect ratio):

$$Vp = l^2 \cdot d_l \qquad (7)$$

As an example, for fluorohectorite nanofiller typical values are l=500nm and d_l=10 nm, thus the average volume of a single lamella is V_p= =2.5·10^{-21} m^3. In the case of 5% wt filler concentration and with ρ_f = 3000 g/l, the number of particles per unit volume, calculated according to (6) is N=9.3·10^{18} m^{-3}. The average distance between the centers of the lamellae (considered as enclosed in spheres, [34]) is D=1/$N^{-1/3}$≈ 475nm, which is much lower than in the case of spherical particles and can reflect particle overlap. This can cause percolation paths, as qualitatively indicated by Fig. 14 and quantitatively estimated as follows.
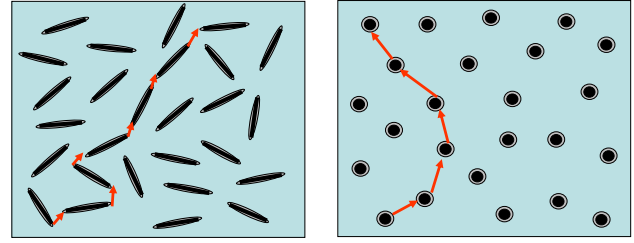

Fig. 14. Sketch of a high- aspect ratio (e.g. fluorohectorite) (a) and low aspect-ratio (e.g. boehmite (b) filled material. The water shells around the nanoparticles are reported in gray. A possible percolation path is indicated by red arrows. Percolation is much more likely for high-aspect ratio particles.

When the distance among the particles is small (below a few tens of nanometers), hopping of electronic carriers between conductive states (i.e. the water shells) is possible. The charge mobility, μ, can be expressed as [34, 40]:

$$\mu = \frac{2kTR}{hE} \cdot e^{\frac{-\Delta U}{kT}} \cdot sinh\left(\frac{q_e ER}{2kT}\right) \cdot e^{-\alpha R} \qquad (8)$$

Where k is the Boltzmann constant, T is the absolute temperature, R is the distance between conductive states, h is the Plank constant, E is the applied electric field, ΔU is the barrier potential between the conductive states, q_e is the electron charge and α is the inverse localization length which describes the exponential decay of the electronic wave function. The charge mobility is plotted in Fig. 15 as a function of R for T=300 K, ΔU=0.5 eV, α=10^9 m^{-1} and E=40kV/mm, corresponding to the average value of field used in the DC tests. As can be seen, the charge mobility has a maximum in correspondence of R=5nm and decreases to much lower values for R> 50 nm. This result indicates that that hopping between the conductive water shells is possible in the case of the high-aspect ratio particles, in which the distance between the particles can be of a few nanometers. On the contrary, hopping among the water shells surrounding low aspect-ratio particles is very unlikely, since the average distance among them is 360 nm.
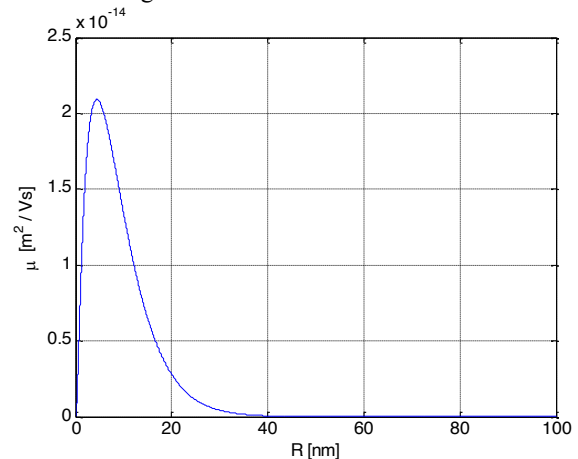

Fig. 15. Charge mobility calculated according to (8) as a function of the distance between localized states R.

Therefore, the probability of having two adjacent lamellae at a distance of a few nanometers, and thus of having a local percolation process, can depend on the aspect ratio of the particles.

A stochastic approach supporting this empirical result can be based on Monte Carlo simulations of the hopping probability among adjacent nanoparticles, which can be

calculated as the product of the probability of extracting the electron from the nanoparticle/polymer interface, P_{extr} and the probability of the transport process, P_{trans}, through the polymer from the polymer/nanoparticle interface to the next nanoparticle. The probability of hopping between adjacent nanoparticles is calculated operatively on the basis of the length of the hopping path and of the component of the electric field along the path (as mentioned earlier the scalar product between the electric field vector and the hopping path was used for the calculation). Then the values of probability obtained per each adjacent nanoparticle are compared and the nanoparticle with the highest probability is selected for being part of the path. It should be noted that since *a)* P_{extr} is a constant term which does not depend on the aspect ratio of the nanoparticles and *b)* since we are interested in the trend of the total probability as a function of the aspect ratio rather than its absolute value, P_{extr} can be neglected, as first approximation. According to then suggestion provided by Len Dissado, the Mott law is used to calculate the probability of each hopping event, that is [41]:

$$P(R) = exp\left[-\left(\alpha R \cos\vartheta + \frac{\Delta W - q_e \cdot E \cdot R \cos\vartheta/2}{kT}\right)\right] \quad (9)$$

Where $R\cos\vartheta$ is the component of the hopping path along the direction of E, ΔW is the height of the barrier potential of the hopping process.

Fig. 16 reports the statistical distribution of the probability exponents obtained from simulations of a 10x10 array of particles, analysing two different aspect ratios of the nanoparticles, i.e. 10 and 100. From filler concentration (5%wt), filler density (ρ_f = 3000g/l) and matrix density (ρ_m = 1400g/l) the distance among the lamella centres, b = 0.5 μm, can be calculated as explained above. There are clearly two populations of probability exponents, correlated with the aspect ratio and the message is that the average exponent values decrease significantly (from 2900 to 1250) when the aspect ratio increases (from 10 to 100), thus resulting in a large increase of the charge transfer probability. Carrying on several simulations with different nanoparticle aspect ratios (fixing the nanoparticle long dimension, l, the thickness, d, is provided by the aspect ratio), the average probability can be evaluated per each set of m simulations and plotted as a function of the aspect ratio, Fig. 17. As can be seen, the probability exponent increases of about 7 times if the aspect ratio changes from 1 to 500, thus providing large raise of charge transfer probability, and, therefore, percolation likelihood.
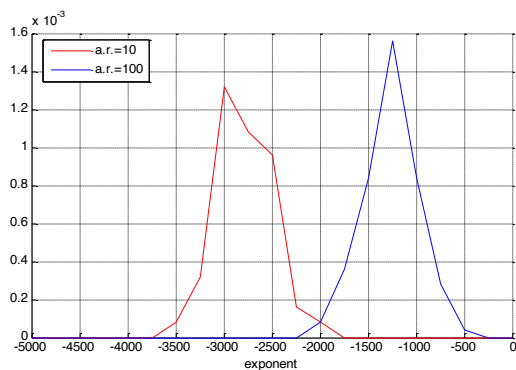
humidity absorbed by the nanomaterial, in fact, nanofiller with large aspect ratio (like layered silicates) can worsen noticeably the electrical performance of the material. Other nanofillers with smaller aspect ratio (e.g. SiO_2 or boehmite) do not behave so negatively in humid environment. Thus, for example, what can improve mechanical properties and partial discharge resistance may not be good as well for some electrical properties, including losses and design field of insulation.
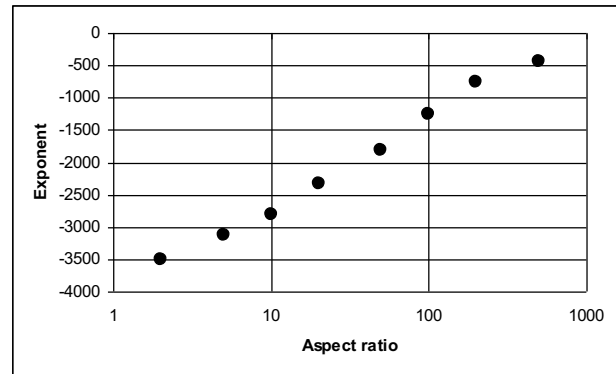

Fig. 17. Behaviour of the probability exponent, eq. (9), as a function of the aspect ratio with $\alpha=10^9$ m^{-1}.

These results can serve as a caution for dielectric application. Electron percolation must be avoided to maintain electric integrity, but this raises the traditional challenge of balancing electrical and thermal properties. Phonon percolation promotes effective heat transfer. Comprehensive research [42] has made it clear that meeting the thermal, mechanical and electrical requirements of an insulation system cannot be met by selectively optimizing one parameter. The material design for one property, e.g., thermal conductivity, can have a negative impact on the breakdown strength.

The light shed by types of research as that summarized above brought more clear directions into designing nanostructured materials tuned to specific applications, thus abandoning the too- bright dream to have discovered the magic powder able to elevate any dielectric property.

5. Conclusions

Quid faciat laetas segetes
quo sidere terram vertere, Maecenas,
ulmisque adjungere vitis conveniat,
que cura boum,
qui cultus habendo sit pecori, apibus
quanta experientia parcis,
Hinc canere incipiam [43].

What makes the crops joyous,
beneath what star, Maecenas,
it is well to turn the soil, and wed vines to elms,
what tending the cattle need, what care the herd in breeding,
what skill the thrifty bees,
hence shall I begin my song.

This is what Vergilius wrote 2050 years ago, and it could still summarize our challenge in science and research, i.e. hard work, imagination, courage, skill, humbleness and funding (even if we can see hardly Mecanates nowadays). We can then try to catch our fireflies to light up our summer nights

Fig. 16. Probability density distributions of the exponent of eq. (9) for aspect ratio (a.r.) of the nanoparticles = 10 and 100.

This demonstrates that the aspect ratio of the nanoparticles can play a significant role in modifying the properties of insulation nanocomposites. In the presence of

and … may the Gods be kind to us 神々が私たちに親切になりますように(Kamigami ga watashitachi ni shinsetsu ni narimasu yō ni).

_____

References

1. T. Tanaka. A. Greenwood, Advanced Power Cable Technology, United States (1983).
1. K. Sato, T. Hikata, H. Mukai, M. Ueyama, N. Shibuta, T. Kato, T. Masuda, M. Nagata, K. Iwata, and T. Mitsui, IEEE Trans. Magn. **27**, 1231 (1991).
2. T. Shibata, M. Watanabe, C. Suzawa, S. Isojima, J. Fujikami, K. Sato, H. Ishii, S. Honjo, and Y. Iwata, IEEE Trans. Power Delivery, **14**, 182 (1999).
3. M. M. Rahman, M. Nasi, IEEE Spectrum, **34**, 31 (1997).
4. A. Narlikar, Studies of High-Temperature Superconductors - Advances in Research and Application: The BSCCO System-II, Nova Science Publishers Incorporated, Hauppauge, NY (2001).
5. N. Kelley, M. Nassi, L. Masur, IEEE PES Winter Meeting, **2**, 448 (20).
6. R. G. Jones et al., Phys. Lett. **24**, 318 (1967).
7. W. H. Warnes and D. C. Larbalestier, Cryogenics, **26**, 643 (1986).
8. G. C. Montanari, I. Ghinello, L. Gherardi, P. Caracino, IEEE Trans. Appl. Supercond. **6**, 132 (1996).
9. M. G. Kendall and A.Stuart, "The advanced theory of statistics", 1, 2 and 3, Griffin Publ., London (1983).
10. M. Cacciari, G. Mazzanti and G. C. Montanari, IEEE Trans, Dielctr. Electr. Insul. **3**, 18 (1996).
11. G. C. Montanari, I. Ghinello, L. Gherardi, P. Caracino, IEEE Trans. Appl. Supercond. **7**, 1303 (1997).
12. D. Fabiani, G.C. Montanari, IEEE Trans. Appl. Supercond. **14**, 1915 (2004).
13. G. C. Montanari and L. Simoni, IEEE Trans. Electr. Insul., **28**, 755 (1993).
14. D. Fabiani, G.C. Montanari, IEEE Trans. Appl. Supercond. **14**, 1848 (2004).
15. S. Komarneni, J. Mater. Chem., **2**, 1219 (1992).
16. E.P. Giannelis, Adv. Mater., **8**, 29 (1996).
17. T. J. Lewis, IEEE Trans. Dielectr. Electr. Insul. **1**, 812 (1994).
18. P. C. Irwin, Y. Cao, A. Bansal and L. Schadler, Proc.IEEE-CEIDP, **2B-14**, 120 (2003).
19. J.K. Nelson, J.C. Fothergill, L.A. Dissado and W. Peasgood, Annu. Rep. - Conf. Electr. Insul. Dielectr. Phenom. (CEIDP), Cancun, Mexico, pp. 295-298 (2002).
20. C. Zilg, D. Kampfer, R. Thomann, R. Mulhaupt, G.C. Montanari, IEEE Conf. Electr. Insul. Dielectr. Phenom. (CEIDP), Albuquerque, USA, pp. 546-550 (2003).
21. G. C. Montanari, D. Fabiani, F. Palmieri, D. Kaempfer, R. Thomann and R. Mülhaupt, IEEE Trans. Dielectr. Electr. Insul. **11**, 754 (2004).
22. T. Tanaka, G. C. Montanari and R. Mulhaupt, IEEE Trans. Dielectr. Electr. Insul. **11**, 763 (2004).
23. M. F. Frechette, M. L. Trudeau, H. D. Alamdar and S. Boily, IEEE Trans. Dielectr. Electr. Insul. **11**, 808 (2004).
24. Y. Cao, P. C. Irwin and K. Younsi, IEEE Trans. Dielectr. Electr. Insul. **11**, 797 (2004).
25. M. Roy, J. K. Nelson, R. K. MacCrone, L. S. Schadler, C. W. Reed and R. Keefe, IEEE Trans. Dielectr. Electr. Insul. **12**, 629 (2005).
26. T.Tanaka, IEEE Trans. Dielectr. Electr. Insul., **12**, 914 (2005).
27. A. Cavallini, D. Fabiani, G.C. Montanari, IEEE Conf. Electr. Insul. Dielectr. Phenom. (CEIDP), Vancouver, Canada, pp. 256-259 (2007).
28. T. Tanaka, IEEE Conf. Electr. Insul. Dielectr. Phenomena (CEIDP), Kansas City, MO, USA, pp. 298-301 (2006).
29. A. Saccani, A. Motori, F. Patuelli, G.C. Montanari, IEEE Trans. Dielectr. Electr. Insul. **14**, 689 (2007).
30. T. Imai, T. Tanaka, J. Inst. Electr. Eng. Jpn. **134**, 161 (2014).
31. C. Zou, J. C. Fothergill, S. W. Rowe, IEEE Trans. Dielectr. Electr. Insul. **15**, 106 (2008).
32. D. Fabiani, G. C. Montanari, L. Testa, R. Schifani, F. Guastavino, F. Bellucci, F. Deorsola, Int. Symp. Electr. Insul. Mater. (ISEIM), Yokkaichi, Japan, pp. 510-513, 2008.
33. D. Fabiani, G. C. Montanari, L. Testa, IEEE Trans. Dielectr. Electr. Insul. **17**, 221 (2010).
34. S. Ray, M. Okamoto, Progress in Polymer Science, **28**, 1539 (2003).
35. T. Tanaka, A. Bulinski, J. Castellon, M. Frechette, S. Gubanski, J. Kindersberger, G. C. Montanari, M. Nagao, P. Morshuis, Y. Tanaka, S. Pelissou, A. Vaughan, Y. Ohki, C. W. Reed, S. Sutton, S. J. Han, IEEE Trans. Dielectr. Electr. Insul. **18**, 1484 (2011).
36. G. C. Montanari, P. Seri, M. Ritamäki, K. Lahti, I. Rytöluoto, M. Paajanen, IEEE Int. Conf. Prop. Appl. Dielectr. Mater. Xi'an, Cina, pp. 41-44 (2018).
37. T. Tanaka, IEEE Conf. Electr. Insul. Dielectr. Phenomena (CEIDP), Kansas City, MO, USA, pp. 298-301 (2006).
38. T. J. Lewis, IEEJ Trans. Fund. Mat. **126**, 1020 (2006).
39. L. A. Dissado and J. C. Fothergill. Electrical Degradation and Breakdown in Polymers. The Institution of Engineering and Technology, Michael Faraday House, Six Hills Way, Stevenage SG1 2AY, UK (1992).
40. N. F. Mott and R. W. Gurney, Electronic Processes in Ionic Crystals, Oxford Clarendon, U.K. (1948).
41. Lokanathan M, Acharya PV, Ouroua A, Strank SM, Hebner RE, Bahadur V. Proc. IEEE. **109**, 1364 (2021).
42. P. V. Maro, Georgics, Cambridge University Press, Cambridge, UK (1988).